Infrared Physics & Technology 52 (2009) 252–256

Contents lists available at ScienceDirect

Infrared Physics & Technology

journal homepage: www.elsevier.com/locate/infrared

Quantum dot nanostructures for multi-band infrared detection

A.G.U. Perera [a,*,1], G. Ariyawansa [a], G. Huang [b], P. Bhattacharya [b]

[a] Department of Physics and Astronomy, Georgia State University, Atlanta, GA 30303, USA
[b] Solid State Electronics Laboratory, Department of Electrical Engineering and Computer Science, University of Michigan, Ann Arbor, MI 48109-2122, USA

ARTICLE INFO

Article history:
Available online 8 September 2009

PACS:
73.21.La
85.60.Bt
85.60.Gz
85.35.Be

Keywords:
Quantum dot
Infrared detectors
Super-lattice
Resonant tunneling
Bias-selectable
Multi-band

ABSTRACT

A dual-band (two-color) tunneling-quantum dot infrared photodetector (T-QDIP) structure, which provides wavelength selectivity using bias voltage polarity, is reported. In this T-QDIP, photoexcitation takes place in InGaAs QDs and the excited carriers tunnel through an AlGaAs/InGaAs/AlGaAs double-barrier by means of resonant tunneling when the bias voltage required to line up the QD excited state and the double-barrier state is applied. Two double-barriers incorporated on the top and bottom sides of the QDs provide tunneling conditions for the second and the first excited state in the QDs (one double-barrier for each QD excited state) under forward and reverse bias, respectively. This field dependent tunneling for excited carriers in the T-QDIP is the basis for the operating wavelength selection. Experimental results showed that the T-QDIP exhibits three response peaks at ~4.5 (or 4.9), 9.5, and 16.9 μm and selection of either the 9.5 or the 16.9 μm peak is obtained by the bias polarity. The peak detectivity (at 9.5 and 16.9 μm) of this detector is in the range of $1.0–6.0 \times 10^{12}$ Jones at 50 K. This detector does not provide a zero spectral crosstalk due to the peak at 4.5 μm not being bias-selectable. To overcome this, a quantum dot super-lattice infrared photodetector (SL-QDIP), which provides complete bias-selectability of the response peaks, is presented. The active region consists of two quantum dot super-lattices separated by a graded barrier, enabling photocurrent generation only in one super-lattice for a given bias polarity. According to theoretical predictions, a combined response due to three peaks at 2.9, 3.7, and 4.2 μm is expected for reverse bias, while a combined response of three peaks at 5.1, 7.8, and 10.5 μm is expected for forward bias.

1. Introduction

The spectral features of an object provide a measure of its temperature or its material composition. An infrared (IR) detector or a camera [1] captures the intensity contrast of the scene. The development of detectors with multi-band characteristics [2,3] and the ability to select spectral bands will be an important achievement in the field of IR detector technology. Applications of such detectors include land-mine detection [4], missile-warning sensors [5], identification of muzzle flashes from firearms [6], and space situational awareness [7]. In addition to defense, this type of IR detectors will be useful in surveillance, geology, agriculture, material classification, disaster relief, oceanography, etc. Moreover, weather satellites benefit from multi-band detectors, while in Astronomy, 2–14 μm imaging will be useful to understand the structure of planetary nebula [8].

One of the major constraints associated with multi-color detectors is the inability to select response peaks or wavelengths without using optical filters and multi-terminal electrical contacts on the detector. The use of optical filters, in addition to reducing the radiation transmission, makes the detector system bulky and complicated. Having multiple electrical contacts on the detector requires sophisticated processing techniques. To avoid these drawbacks, quantum dot infrared photodetectors (QDIPs) were studied, which provide dual-band detection capability with a selection of the operating wavelength by alternating the applied bias voltage polarity. Here, two quantum detector structures: tunneling-quantum dot (T-QDIP) and super-lattice quantum dot infrared photodetector (SL-QDIP) are presented discussing their device physics concepts and experimental results.

2. Bias-selectable Three-color T-QDIP

A resonant tunneling mechanism was used in T-QDIPs in order to develop low dark current room temperature detectors [9] and terahertz detectors [10]. A typical T-QDIP consists of $In_{0.4}Ga_{0.6}As$ QDs embedded in an AlGaAs/GaAs quantum well (QW) coupled

* Corresponding author.
E-mail address: uperera@gsu.edu (A.G.U. Perera).
[1] Also at NDP optronics LLC.

1350-4495/$ - see front matter © 2009 Elsevier B.V. All rights reserved.
doi:10.1016/j.infrared.2009.09.002

to an AlGaAs/InGaAs/AlGaAs double-barrier (DB). The photocurrent generated by transitions from states in the QD to a state in the QW (the resonant-state) can be collected through the double-barrier by resonant tunneling, while the double-barrier system blocks the majority of the carriers contributing to the dark current (carriers excited to any state other than the resonant-state in the QW). This leads to low dark current and increased operating temperatures. In addition, narrow spectral bands can also be obtained by using tight resonant conditions. Following this concept, successful results have been reported for a room temperature T-QDIP [9] showing dual-band response at wavelengths of ~6 and ~17 μm, and a THz T-QDIP [10] operating at 6 THz (50 μm) at 150 K. While the primary aim of using resonant tunneling was to lower dark current, this concept can also be used to obtain electric field dependent wavelength selectivity for a multi-color T-QDIP. Here, a three-color T-QDIP detector (4.5–4.9, 9.5, and 16.9 μm), providing wavelength selection capability for the two peaks at 9.5 and 16.9 μm, is discussed.

The structure of the three-color T-QDIP grown by molecular beam epitaxy (MBE) is shown in Fig. 1. The major modification compared to the previous room temperature T-QDIP is that two double-barriers are integrated on both sides of QD layers in order to introduce different tunneling conditions for photo-carriers transporting in the two directions. The active region consists of pyramidal-shape $In_{0.4}Ga_{0.6}As$ QDs sandwiched between two double-barriers that consist of an $In_{0.1}Ga_{0.9}As$ quantum well between 30 Å thick $Al_{0.2}Ga_{0.8}As$ barriers. The widths of the $In_{0.1}Ga_{0.9}As$ wells in the bottom- and top-double-barrier systems (BDB and TDB) were 60 and 40 Å, respectively. There were 10 periods of these QDs coupled with double-barriers and each period was separated with an undoped 400 Å thick GaAs layer. The GaAs and AlGaAs layers were grown at 610 °C. The $In_{0.4}Ga_{0.6}As$ QDs were grown at 500 °C on top of a wetting-layer (WL) with a thickness of three monolayers. QDs with height and base dimensions of ~6 and ~20 nm, respectively, were *n*-doped to 1×10^{18} cm^{-3} using Si as the dopant, while the GaAs bottom- and top-contact layers were doped to 2×10^{18} cm^{-3}. Vertical circular mesas for top illumination were fabricated by standard photolithography, wet chemical etching and contact metallization techniques. The highly doped *n*-type top ring contact and the bottom contact were formed by evaporated Ni/Ge/Au/Ti/Au with thickness of 250/325/650/200/2000 Å. The radius of the optically active area of a processed device was 300 μm. Devices for testing were mounted onto chip carriers with epoxy and gold wire contacts were made to connect the device to the chip carrier leads.

A theoretical analysis was carried out prior to the growth of this detector structure as a part of the design process. The calculation of the QD energy levels was carried out using an 8-band **k.p** model [11]. The energy states in the double-barriers and well including the wetting-layer were calculated by solving the one dimensional (1D) Schrödinger equation, while the transmission probability for these states is calculated using the transfer matrix method [12]. The conduction band profile for this T-QDIP is shown in Fig. 2 for (a) zero, (b) forward, and (c) reverse applied bias conditions. The calculated energy levels in the QDs and double-barrier systems are also shown in this figure. The bound states in the QDs are located at −0.156, −0.065, and −0.026 eV (ground, first excited, and second excited state, respectively) with respect to the GaAs conduction band edge. The energy states in the WL and the double-barriers are indicated by the dashed line and short dashed lines, respectively. Unlike the QD states, the states in the DBs and WL can extend beyond their local regions. As shown in Fig. 2a, photo-absorption takes place in the QDs and electrons are excited from the QD ground state to the first QD excited state (transition 3 with ΔE ~91 meV), to the second QD excited state (transition 2 with ΔE ~130 meV), or to the WL state (transition 1). These transitions correspond to three response peaks at 13.6, 9.5, and ~5 μm, respectively. As shown in Fig. 2b, the second QD excited state will lineup with the TDB state under a specific forward bias (top-contact is positive) value, providing maximum tunneling probability for the carriers excited to the second QD state. This leads to a photoresponse at 9.5 μm. Similarly, as shown in Fig. 2c, under a specific reverse bias value (bottom-contact is positive), the first QD excited state will overlap with the lower BDB, leading to a response peak at 13.6 μm (ΔE = 91 meV). However, the carriers excited to the WL state can tunnel through either barrier under any bias condition. Hence, a short wavelength peak in the 4.5–4.9 μm range is also expected, which will not be controlled by the applied bias.

The dark current of the T-QDIP was measured at different temperatures and the dark current density at 50, 200, 240, and 300 K are shown in Fig. 3. The flat region at low bias is due to the instrument current limit at 10^{-10} A. The dark current densities at 80 K and 300 K are 4×10^{-8} A/cm^2 at ±4 V and 8×10^{-4} A/cm^2 at ±2 V, respectively. As expected, this detector shows low dark current characteristic compared to other QDIPs [13]. The measured and calibrated spectral response with bias at 50 K and 80 K are shown in Fig. 4a and b, respectively. Under forward bias (2 V),

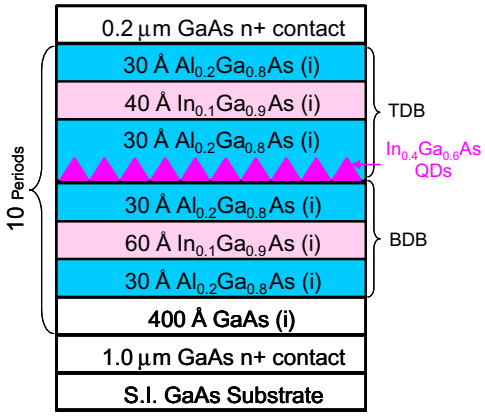

Fig. 1. A schematic diagram of the three-color T-QDIP structure grown by MBE. $In_{0.4}Ga_{0.6}As$ QDs are placed in between two $Al_{0.2}Ga_{0.8}As/In_{0.1}Ga_{0.9}As/Al_{0.2}Ga_{0.8}As$ double-barriers (top- and bottom double-barriers indicated by TDB and BDB, respectively). QDs with height and base dimensions of the ~6 and ~20 nm, respectively, were *n*-doped to 1×10^{18} cm^{-3}. The GaAs bottom- and top-contact layers were *n*-doped to 2×10^{18} cm^{-3}.

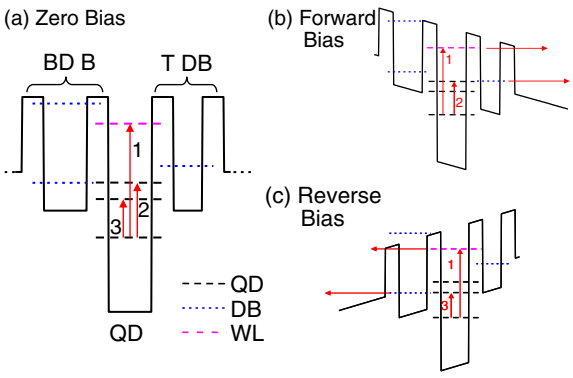

Fig. 2. The conduction band profile of the three-color T-QDIP structure under (a) zero, (b) forward, and (c) reverse applied bias conditions. The calculated bound state locations in QDs, wetting-layer (WL), and double-barriers are indicated by black dashed lines, pink dashed lines, and blue short dashed lines, respectively. (For interpretation of the references to color in this figure legend the reader is referred to the web version of the article.)

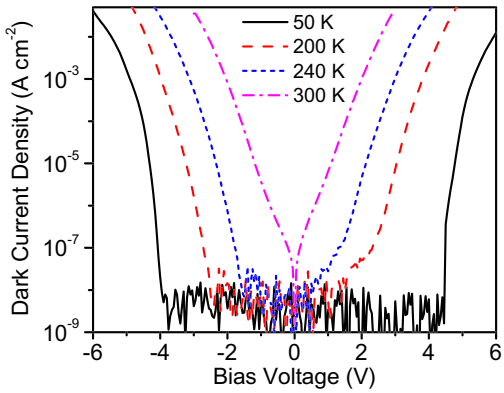

Fig. 3. Dark current characteristics of the three-color T-QDIP at different temperatures.

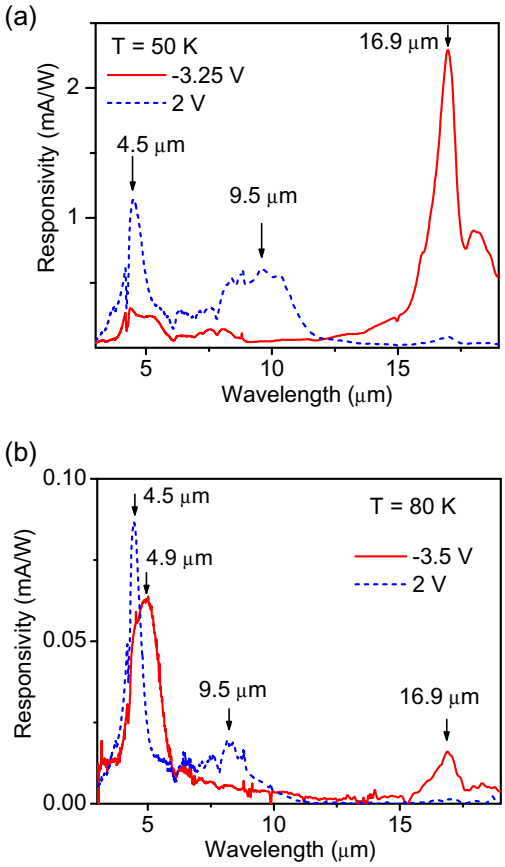

Fig. 4. Calibrated spectral responsivity of the three-color T-QDIP at (a) 50 K and (b) 80 K under 2 and −3.25 V bias. A peak at 9.5 μm is observed for forward bias (2 V), while a peak at 16.9 μm is observed for reverse bias (−3.5 V). The peak at 4.5/4.9 μm due to transitions to the wetting-layer can be observed for both forward and reverse bias.

two peaks were observed at 4.5 and 9.5 μm due to transitions from the QD ground state to the WL state and to the second QD excited state, respectively. Under reverse bias (−3.25 V), two peaks were observed at 4.9 and 16.9 μm due to transitions from the QD ground state to the WL state and the first QD excited state. As predicted before, the peaks at 9.5 and 16.9 μm show a good selectivity with bias, while 4.5 (or 4.9) μm was apparent at any bias. The shift of this peak is also consistent with theoretical prediction, which showed ΔE = 264 and 249 meV for transition 1 for forward and reverse bias, respectively. Using the responsivity and the measured noise current density spectra, the detectivity values at 50 K for the peaks at 4.5 (at 2 V), 9.5 (at 2 V), and 16.9 μm (at −3.25 V) are 3.0, 1.6, and 6.0×10^{12} Jones, respectively.

3. SL-QDIP Responding in the Atmospheric Windows

To achieve complete bias-selectability of the dual-band response with minimal spectral crosstalk, a SL-QDIP structure similar to super-lattice quantum well infrared photodetector (SL-QWIP) structures [14] was developed and is discussed in this section. One major issue associated with the T-QDIP is that the WL transition peak cannot be controlled using bias, hence, the spectral crosstalk cannot be eliminated. While SL-QDIP overcomes that issue, it also provides response wavelength tunability at the detector design stage by changing the mini-bands without changing the QD size. Unlike reducing the QD size, mini-bands can be easily adjusted by changing the quantum well widths. A SL-QDIP was designed, fabricated, and tested and the results indicate the feasibility of using SL-QDIP structures for future wavelength controllable multi-color detector development.

A schematic diagram of the SL-QDIP structure grown by MBE is shown in Fig. 5. This consists of two QD-SLs (top- and bottom QD-SL) separated by a graded AlGaAs barrier, which are sandwiched in two highly doped contact layers. The two QD-SLs are identical and consist of self-assembled $In_{0.4}Ga_{0.6}As$ QDs placed in a super-lattice made of five periods of 90 Å GaAs/30 Å $Al_{0.4}Ga_{0.6}As$ quantum wells (see Fig. 5). Similar to the T-QDIP, QDs have height and base dimensions of ~6 and ~20 nm, respectively, and were *n*-doped to 1×10^{18} cm^{-3} using Si. The two SLs are separated by a thick $Al_xGa_{1-x}As$ graded barrier (Al fraction: 0.09 → 0.3). The growth parameters of the layers are similar to those of the T-QDIP discussed before. While this structure consists of one active period (top-QD-SLs/graded barrier/bottom-QD-SL), it is also possible to use multiple periods, which can be expected to show high performance. However, the number of periods has to be determined to optimize the performance, taking growth issues into account.

The conduction band profile for this structure under forward and reverse bias with the bound state in QDs (E_0, E_1, and E_2) and mini-bands (M_1 and M_2) in both SLs are shown in Fig. 6. These bound states in the QDs (E_0, E_1, and E_2) are located at −0.156, −0.065, and −0.026 eV with respect to the GaAs conduction band edge. The SLs exhibit two mini-bands located at 0.093 and 0.269 eV with respect to the GaAs conduction band edge. In both SLs, the effect of the WL has been taken into account. As the QDs are doped and the highly doped GaAs contact layers are separated only by a thin AlGaAs layer, all the QD energy states are filled with carriers. The detection mechanism includes transitions of electrons from all QD states (E_0, E_1, and E_2) to the mini-bands in the SLs. Each SL would lead to a combined response peak as a result of three electronic transitions (combination of three peaks). In this design, the most important fact is that only one SL becomes active for photocurrent generation under a given bias direction (forward or reverse). Under reverse bias (top-negative), a combined response due to three peaks at 2.9, 3.7, and 4.2 μm is expected due to electronic transitions from QD states to the upper mini-band (M_2). The carriers excited to the lower mini-band (M_1) do not contribute to the photocurrent because of the blocking by the AlGaAs barrier. Similarly, under forward bias (top-positive), a combined response of three peaks at 5.1, 7.8, and 10.5 μm is expected due to electronic transitions from QD states to the lower mini-band state (M_1). Although the response of this detector is not confined purely in the 3–5 and 8–14 μm atmospheric windows, considering the current growth capabilities, it can be further modified to obtain responses solely in the two atmospheric windows.

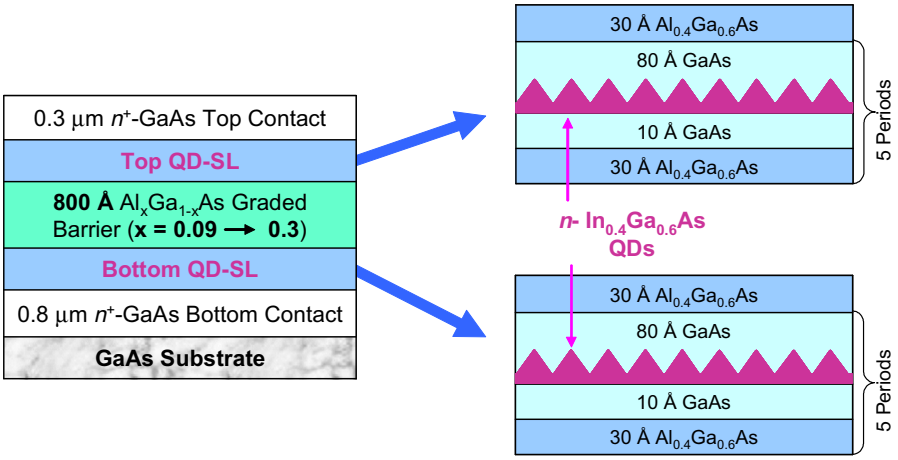

Fig. 5. Schematic diagram of the SL-QDIP detector. The two SLs, each of which consists of $In_{0.4}Ga_{0.6}As$ QDs placed in $GaAs/Al_{0.4}Ga_{0.6}As$ super-lattice, are separated by a thick graded AlGaAs barrier. These are then sandwiched between two thick highly doped GaAs layers.

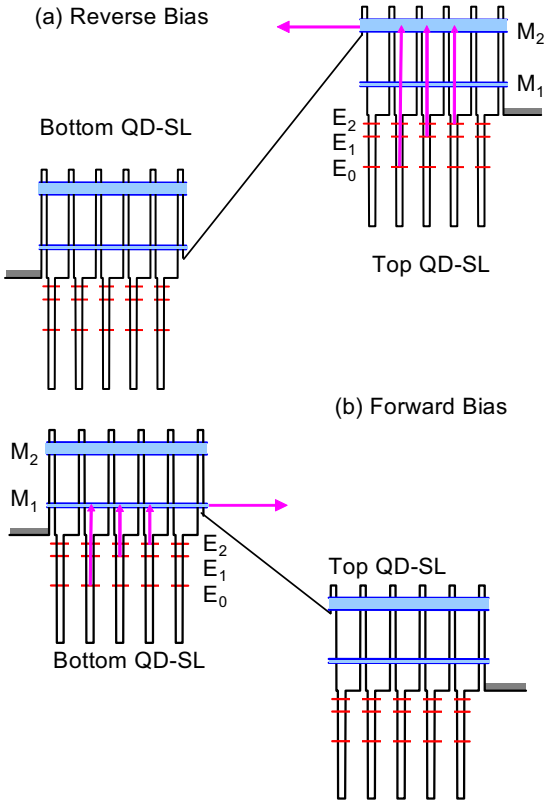

Fig. 6. The conduction band profile under (a) reverse and (b) forward bias conditions. The bound states in QDs (E_0, E_1, and E_2) and mini-bands (M_1 and M_2) in both SLs are also shown. Possible transitions from QD states to mini-bands, leading to spectral response peaks are indicated by vertical arrows.

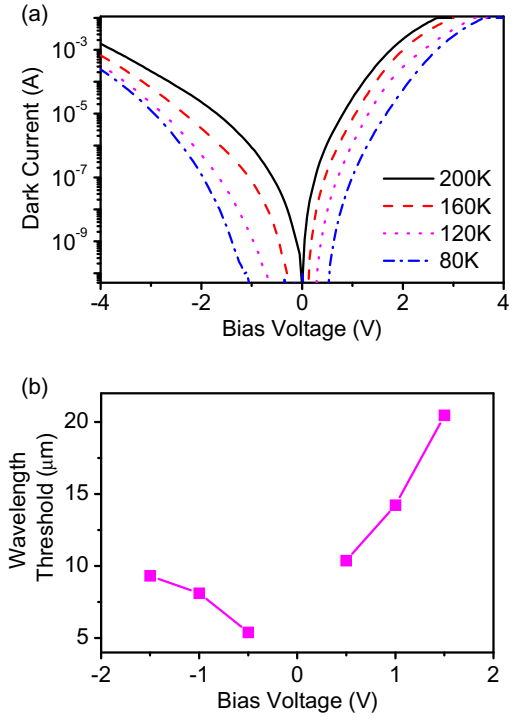

Fig. 7. (a) Dark current characteristics of the SL-QDIP at temperatures between 80 and 200 K. The asymmetry in the IV is due to the difference in the effective barrier seen by the carriers in the two QD-SLs. (b) Variation of the wavelength threshold with bias, which was calculated based on an Arrhenius analysis. The wavelength threshold for low bias agrees well with the experimental results and throughout the full operating bias region, the threshold for forward bias is longer than that of reverse bias, as expected.

Dark current measurement on a processed SL-QDIP detector was performed at different temperatures (see Fig. 7a). The asymmetry in the IV is due to the difference in the effective barrier seen by the carriers in the two QD-SLs. Using the dark current data, an Arrhenius analysis was carried out and the activation energies for different bias voltages were obtained. The variation of the wavelength threshold, which correspond to the activation energy obtained from Arrhenius analysis, with applied bias is shown in Fig. 7b. The wavelength thresholds for low bias (~0.5 V) agree with the theoretically predicted responses, while the wavelength threshold rapidly increases when the bias is increased. This type of effect is expected in Arrhenius analysis if tunneling takes place as opposed to thermal excitations. However, throughout the complete bias region, the threshold for forward bias is longer than that of reverse bias, as expected. The spectral response of this SL-QDIP at 80 K for bias values of −3 V and 1.5 V is shown in Fig. 8. Under reverse bias, a dominant peak at 4.9 μm can be observed. Under forward bias, three peaks with a dominant peak at 7.4 μm are observed. The observed wavelengths of the peaks are in good agreement with the predicted peak locations discussed before. Although

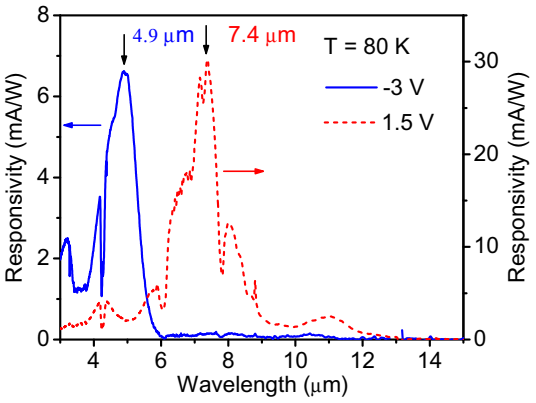

Fig. 8. Spectral response of the SL-QDIP at 80 K under −3 V and 1.5 V bias voltages. The two spectral bands with peak wavelengths at 4.9 μm (at −3 V) and 7.4 μm (at 1.5 V) are due to electronic transitions from QD states to the upper and lower mini-bands, respectively.

the spectral overlap between the two response bands is not zero, it can be reduced by pushing the long wavelength response into the 8–14 μm region, which can be done by adjusting the bottom superlattice parameters.

4. Summary

A bias-selectable T-QDIP with response peaks at 4.5 (or 4.9), 9.5, and 16.9 μm, with a selectivity of the 9.5 and 16.9 μm peaks by alternating the applied bias polarity was presented. A SL-QDIP structure for dual-band detectors with a wavelength selection using applied bias and a reduced spectral crosstalk was investigated. It was theoretically shown that a combined response due to three peaks at 2.9, 3.7, and 4.2 μm for reverse bias and a combined response of three peaks at 5.1, 7.8, and 10.5 μm for forward bias can be obtained for a preliminary SL-QDIP. Wavelength thresholds obtained based on Arrhenius analysis using the dark current of this SL-QDIP has shown a reasonable agreement with the theoretically predicted wavelength thresholds for low applied bias voltages. Furthermore, spectral response measurements on this SL-QDIP have shown promising results with two peaks at 4.9 and 7.4 μm for reverse and forward bias, respectively, which are also in good agreement with theoretical predictions.

Acknowledgement

This work is supported in part by the US Air Force under the STTR Contract No: FA9550-09-C-0106 (NDP Optronics LLC and GSU) and the US NSF Grant ECCS: 0620688 (Univ. Michigan and GSU).

References

[1] A. Rogalski, Optical detectors for focal plane arrays, Opto-Electron. Rev. 12 (2) (2004) 221–245.
[2] S. Krishna, S. Raghavan, G. von Winckel, et al., Three-color (λp1 ~3.8, λp2 ~8.5, and λp3 ~23.2 μm) InAs/InGaAs quantum-dots-in-a-well detector, Appl. Phys. Lett. 83 (14) (2003) 2745–2747.
[3] S. Chakrabarti, X.H. Su, P. Bhattacharya, et al., Characteristics of a multicolor InGaAs–GaAs quantum-dot infrared photodetector, IEEE Photon. Technol. Lett. 17 (2005) 178–180.
[4] A. Goldberg, P.N. Uppal, M. Winn, Detection of buried land mines using a dual-band LWIR/LWIR QWIP focal plane array, Infrared Phys. Technol. 44 (2003) 427.
[5] Filip Neele, Two-color infrared missile warning sensors, SPIE Proc. 5787 (2005) 134.
[6] David B. Law, Edward M. Carapezza, Christina J. Csanadi, et al., DARPA counter-sniper program: phase 1 Acoustic Systems Demonstration results, SPIE Proc. 2938 (1997) 288.
[7] P.M. Alsing, D.A. Cardimona, D.H. Huang, et al., Advanced space-based detector research at the Air Force Research Laboratory, Infrared Phys. Technol. 50 (2007) 89.
[8] M. Meixner, C.J. Skinner, P. Temi, et al., Astrophys. J. 411 (1993) 266.
[9] P. Bhattacharya, X.H. Su, S. Chakrabarti, et al., Characteristics of a tunneling quantum-dot infrared photodetector operating at room temperature, Appl. Phys. Lett. 86 (19) (2005) 191103–191106.
[10] X.H. Su, J. Yang, P. Bhattacharya, et al., Terahertz detection with tunneling quantum dot intersublevel photodetector, Appl. Phys. Lett 89 (2006) 031117.
[11] H. Jiang, J. Singh, Strain distribution and electronic spectra of InAs/GaAs self-assembled dots: an eight-band study, Phys. Rev. B 56 (1997) 4696–4701.
[12] Emmanuel Anemogiannis, Elias N. Glytsis, Senior Member, et al., Quasi-bound states determination using a perturbed wavenumbers method in a large quantum box, IEEE J. Quantum Electron. 33 (1997) 742–752.
[13] G. Ariyawansa, A.G.U. Perera, G.S. Raghavan, et al., Effect of well width on three color quantum dots-in-a-well infrared detectors, IEEE Photon. Technol. Lett. 17 (2005) 1064–1066.
[14] Amlan Majumdar, K.K. Choi, J.L. Reno, et al., Voltage tunable superlattice infrared detector for mid- and long-wavelength detection, Appl. Phys. Lett. 86 (26) (2005) 261110–261113.